

Article

Spatiotemporal Variation and Pattern Analysis of Air Pollution and Its Correlation with NDVI in Nanjing City, China: A Landsat-Based Study

Qianqian Sheng^{1,2,3,4}, Yaou Ji^{1,2,3,4}, Chengyu Zhou^{1,2}, Huihui Zhang^{1,2} and Zunling Zhu^{1,2,3,4,5,*}

¹ College of Landscape Architecture, Nanjing Forestry University, Nanjing 210037, China; qqqs@njfu.edu.cn (Q.S.); jiyao@njfu.edu.cn (Y.J.); zhouchengyu@njfu.edu.cn (C.Z.); zhanghuihui@njfu.edu.cn (H.Z.)

² Co-Innovation Center for the Sustainable Forestry in Southern China, Nanjing Forestry University, Nanjing 210037, China

³ Jin Pu Research Institute, Nanjing Forestry University, Nanjing 210037, China

⁴ Research Center for Digital Innovation Design, Nanjing Forestry University, Nanjing 210037, China

⁵ College of Art and Design, Nanjing Forestry University, Nanjing 210037, China

* Correspondence: zhuzunling@njfu.edu.cn

Abstract: The rapid socio-economic development and urbanization in China have led to a decline in air quality. Therefore, the spatial and temporal distribution patterns of urban air pollution, as well as its formation mechanisms and influencing factors, have become important areas of research in atmospheric environment studies. This paper focuses on nine monitoring sites in Nanjing, where concentration data for six air pollutants and vegetation index data were collected from 2013 to 2021. The objective of this study is to investigate the changes in air pollutants and vegetation index over time and space, as well as their relationship with each other, and to assess the social and environmental impacts of air pollution. The findings reveal a spatial distribution pattern of air pollution in Nanjing that exhibits significant variability, with pollutant concentrations decreasing from the city center towards the surrounding areas. Notably, the main urban area has lower air quality compared to the peripheral regions. The results obtained from best-fit linear regression models and correlation heatmaps demonstrate a strong correlation (coefficient of determination, $R^2 > 0.5$) between the normalized difference vegetation index (NDVI) and pollutants such as SO_2 , NO_2 , $\text{PM}_{2.5}$, PM_{10} , and O_3 within a radial distance of 2 km from the air pollutant monitoring sites. These findings indicate that NDVI can be an effective indicator for assessing the distribution and concentrations of air pollutants. Negative correlations between NDVI and socio-economic indicators are observed under relatively consistent natural conditions, including climate and terrain. Therefore, the spatiotemporal distribution patterns of NDVI can provide valuable insights not only into socio-economic growth but also into the levels and locations of air pollution concentrations.

Keywords: Landsat; NDVI; air pollutants; socio-economic indicators; correlation; China



Citation: Sheng, Q.; Ji, Y.; Zhou, C.; Zhang, H.; Zhu, Z. Spatiotemporal Variation and Pattern Analysis of Air Pollution and Its Correlation with NDVI in Nanjing City, China: A Landsat-Based Study. *Forests* **2023**, *14*, 2106. <https://doi.org/10.3390/f14102106>

Academic Editor: Giacomo Alessandro Gerosa

Received: 25 September 2023

Revised: 17 October 2023

Accepted: 18 October 2023

Published: 20 October 2023



Copyright: © 2023 by the authors. Licensee MDPI, Basel, Switzerland. This article is an open access article distributed under the terms and conditions of the Creative Commons Attribution (CC BY) license (<https://creativecommons.org/licenses/by/4.0/>).

1. Introduction

With the rapid socio-economic development and acceleration of urbanization in China, the issue of air pollution has become increasingly severe, thereby negatively impacting human health, climate, and the sustainable development of cities [1,2]. Mainly, particulate matter (PM) is composed of toxic and harmful substances with high fluidity, which can linger in the atmosphere for extended periods, leading to elevated rates of cardiovascular and respiratory diseases and subsequent morbidity and mortality [3]. To address this severe air pollution problem, the State Council of the People's Republic of China issued the "Action Plan on Prevention and Control of Air Pollution" in September 2013, focusing explicitly on regional air pollution and addressing characteristic pollutants such as inhalable and fine

PM. The plan entails various measures implemented by the Chinese government, including expanding green spaces in urban areas, reducing motor vehicle usage, and increasing clean energy. While the concentrations of air pollutants have reduced to some extent since 2017, exceedances still persist [4]. Nanjing, as the political and cultural hub of East China and a significant center of the eastern Chinese economy, is densely populated with well-developed industrial and agricultural sectors. As of 2021, the permanent population of Nanjing stands at 9.42 million people, with a population density of 1430.6 persons per square kilometer. However, due to rapid economic and population growth, as well as its unique topographical and climatic characteristics, air pollution has become an increasing concern as a widespread issue in Nanjing.

Recent research on regional air pollution has primarily centered on pollution source profiling [5], the relationship between air pollutants and meteorological conditions [6], and the analysis of spatiotemporal variations [7]. Among the meteorological conditions, wind speed is recognized as the primary driver of nitrogen-related air pollution. For example, Banerjee et al. found that atmospheric NO₂ concentration was most influenced by wind speed, followed by the weekly average temperature [8]. Wang et al. reported that higher temperatures, lower surface pressures, and increased wind speed facilitated the dispersion of air pollutants [9]. Jia et al. also emphasized the significant impact of temperature and wind speed on air pollutants [10]. Hrishikesh et al. identified temperature as the main influencing factor, with NO₂ exhibiting a strong correlation with temperature during the monsoon season and humidity during winter [11]. Guo et al. and Cui et al. conducted analyses of air pollution in Nanjing, investigating its spatiotemporal distribution, patterns, and potential sources of pollutants [12,13]. Yuan et al. used machine learning research methods to identify unreasonable NO_x/VOCs emissions reduction as the main factor contributing to the overall extension of ozone in the Pearl River Delta in spring and winter [14]. Ersin, O.O. discovered, through the employment of the dynamic Panel STAR method, that CO₂ emissions are an accumulated process with path-dependence related to the history of emissions and economic growth [15]. However, these studies have primarily focused on the composition, distribution, and concentrations of air pollutants, neglecting the importance of environmental management. Consequently, it is crucial and urgent to conduct research on the spatiotemporal variations of air pollutants, the drivers influencing their concentrations, and environmentally proactive measures to mitigate and prevent these pollutants.

Recent evidence has highlighted the significant role of technological innovations in determining emissions [16]. Currently, two main approaches are employed in studies on air pollution management. The first approach utilizes chemical methods and technologies to address air pollution. For instance, Escobedo et al. employed photocatalytic technology to degrade air pollutants [17]. Wang et al. utilized analytical techniques to investigate dust deposition on streets [18]. Kaya et al. applied green analytical chemistry to mitigate air pollution [19]. The second approach focuses on ecological or environmental management, employing green methods where plants play a vital role in the adsorption, transformation, assimilation, and degradation of air pollutants. This approach also aims to rehabilitate or restore ecosystems affected by air pollution [20]. Plant leaves respond sensitively to air pollution and serve as significant pathways for energy exchange between vegetation and the external environment. Consequently, studying the complex and dynamic interactions between air pollutants and vegetation growth and development has emerged as a prominent research topic. For instance, Freer-Smith et al. demonstrated that plant leaves intercept and immobilize atmospheric PM due to their surface properties [21]. Prusty et al. indicated that plants can absorb air pollutants and reduce atmospheric dust concentrations [22]. Nowak et al. estimated that vegetation in American cities removes a total of 711,000 tons of air pollutants from the atmosphere, providing an economic benefit of USD 3.8 billion. They further revealed that vegetation effectively controls air pollution and enhances the cleanliness of urban environments [23].

Various evaluation indices have been proposed to quantify vegetation, including the normalized difference vegetation index (NDVI), leaf area index, living vegetation volume, green cover index, green visual ratio, and fractional vegetation cover [24–29]. NDVI is derived from a combination of linear and non-linear spectral bands, allowing it to capture the spatiotemporal growth and distribution of vegetation effectively. Furthermore, NDVI demonstrates a strong correlation with vegetation cover and, to some extent, can reflect the socio-economic status of a city [30]. Recent advancements in remote sensing technology have facilitated the exploration of the relationship between urban green spaces on a large scale and the mitigation of urban air pollution [31]. For instance, Sun, S. et al. conducted a correlation analysis between NDVI and air pollution in Beijing, Tianjin, and Hebei, China [32]. Similarly, Huang, G.J. et al. investigated the correlation between PM_{2.5} concentration and fractional vegetation cover in Liupanshui, Guizhou [33]. However, to the best of our knowledge, no studies have been conducted thus far on the spatiotemporal variations and patterns of air pollutants in Nanjing, as well as the impact of vegetation on air pollutants.

The normalized difference vegetation index (NDVI) serves as a standardized vegetation index that effectively characterizes the extent of vegetation coverage within a specific region. By examining the correlation between NDVI and atmospheric pollutants, the development of ecologically responsible urban green spaces with varying purification capacities can be facilitated. This innovative approach utilizes plant-based remediation to control air pollution. Vertical greening, as a viable botanical remediation solution, effectively mitigates the presence of airborne pollutants such as volatile organic compounds (VOCs) and PM, concurrently enhancing urban vegetation coverage within constrained horizontal spaces [34]. Srbinovska et al. reported that vertical greening, through plant-based absorption mechanisms, resulted in a notable reduction of 25.0% and 37.0% in PM_{2.5} and PM₁₀ levels, respectively, thereby affirming its capacity to sequester deleterious fine particulate matter [35]. Additionally, Pettit et al. discerned the capacity of vertical greening in purifying NO₂ and O₃ emissions from combustion by-products, registering purification rates of 121 and 50 m³/(h·m²) for these pollutants, respectively [36]. These findings are of considerable significance for urban landscaping, environmental planning, and the construction of ecological environments. Air pollution can cause direct and indirect adverse effects on fauna, flora, and human health on a regional scale, as seen in Iran [37]. Furthermore, it exerts a significant socio-economic impact on both public health and photovoltaic energy efficiency [38]. Therefore, the objective of this study is to analyze the spatiotemporal variations and patterns of six air pollutants (SO₂, NO₂, CO, O₃, PM_{2.5}, and PM₁₀) in relation to NDVI in Nanjing from 2013 to 2021 while also exploring the spatiotemporal relationships among air pollutants, NDVI, and socio-economic indicators. The outcomes of this study provide insights into sustainable development strategies and practices for governing Nanjing, as well as macro-economic regulation and environmental management.

2. Materials and Methods

2.1. Study Region

Nanjing, the capital of Jiangsu Province, is situated in eastern China downstream of the Yangtze River. It serves as a catalyst for the development of central and western China, radiating from the Yangtze River Delta. Nanjing resides in the Nanjing–Zhenjiang–Yangzhou Hilly Region, characterized by predominantly flat land, low mountains, and hills, with a diverse array of land uses and covers [39]. Surrounded by mountains on three sides and the river on the remaining side, Nanjing boasts an expansive area of mountains and forest vegetation, forming the foundational framework of its green space system [40]. This study focuses on nine air quality monitoring stations located across different districts in Nanjing, as detailed in Table 1.

Table 1. Presents the latitude and longitude coordinates for the nine air quality monitoring sites.

Station	District	Latitude	Longitude
Caochangmen	Jiangdong Street, Gulou District	32.05528	118.754
Shanxi Road	Ninghai Road Street, Gulou District	32.07014	118.7832
Maigaoqiao	Maigaoqiao Street, Qixia District	32.1064	118.8083
Xianlin University City	Xianlin Street, Qixia District	32.10135	118.9105
Pukou	Jiangpu Street, Pukou District	32.0878	118.626
Olympic Sports Center	Xinglong Street, Jianye District	32.00726	118.7422
Zhonghuamen	Zhonghuamen Street, Qinhuai District	32.01267	118.7817
Xuanwu Lake	Xuanwu Gate Street, Xuanwu District	32.07545	118.8
Ruijin Road	Ruijin Road Street, Qinhuai District	32.03225	118.8058

2.2. Data Sources

For this study, satellite images from the Landsat 8 Operational Land Imager (OLI) were employed. These images consist of nine spectral bands with a spatial resolution of 30 m, along with a 15 m panchromatic band. The coverage of the imagery spanned an area of 185×185 km. These image data were acquired from the Landsat 8 dataset, which is available through the Resources and Environmental Science and Data Center of the Chinese Academy of Sciences (<https://www.resdc.cn/>, accessed on 16 December 2022). The dataset encompasses the period from 2013 to 2021.

In this study, we employed index calculation techniques and utilized the ENVI 5.3 software, developed by Harris Geospatial, to combine and overlay data from various bands of Landsat 8 spanning the period from 2013 to 2021 in Nanjing. Through index calculation, we derived mean values of NDVI, the ratio vegetation index (RVI), and the green vegetation index (GVI) for the spring, summer, autumn, winter, and annual periods. The analysis primarily focused on the NDVI, air pollutants, and socio-economic data from the summer and winter seasons. Statistical methods were applied to determine the average NDVI values within different buffer zones surrounding each air quality monitoring site.

In this study, the nine monitoring sites served as central points for analysis. For the monitoring sites in the city center, a radial range of 100, 200, 300, 400, and 500 m was selected due to their relatively short distances. On the other hand, the monitoring sites in suburban areas were chosen with radial ranges of 500 m, 1 km, 2 km, 4 km, 8 km, and 16 km as they were spatially further apart. Figure 1 demonstrates that the selection of these ranges ensured that the surface feature categories and NDVI values remained representative, avoiding issues of being too close or too far apart.

Meter-level accurate DEM data were acquired from the Google Maps Elevation API (Figure 2), offering a spatial resolution of 5 m. To generate a Nanjing DEM with precise geographic information, the obtained DEM data underwent processing in ArcGIS 10.8. This involved mask extraction, spatial adjustment, and coordination system specification, resulting in an accurate representation of Nanjing's terrain. Socio-economic data, including industrial gross value added, GDP per capita, and other relevant information, were sourced from the statistical yearbooks of Nanjing covering the period from 2013 to 2019 [41].

2.3. Data Processing

2.3.1. Determination of NDVI, RVI, and GVI Values

For this study, monitoring points near the city center of Nanjing, specifically along the river basin, were carefully selected. Each monitoring point had a radius ranging from 100 m to 32 km. Among these points, Caochangmen, Shanxi Road, Maigaoqiao, the Olympic Sports Center, the Zhonghuamen, Ruijin Road, and Xuanwu Lake had radii varying from 100 m to 2 km. On the other hand, Pukou and Xianlin University City had radii ranging from 2 km to 32 km. This selection ensured that the indicators obtained from each data point were representative [32]. Using ArcGIS 10.8 software, we calculated various indicators, such as NDVI, RVI, and GVI, within the coverage zones of these monitoring.

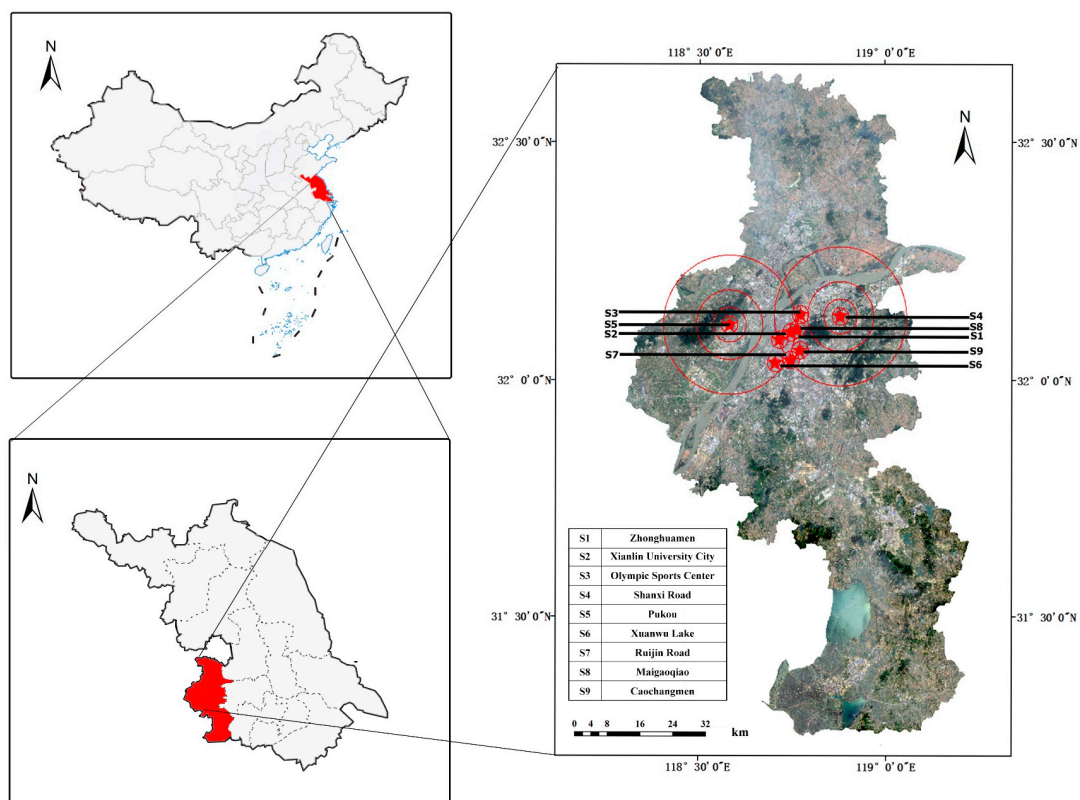


Figure 1. The geographical coordinates of the nine air quality monitoring points located in Nanjing, Jiangsu Province, China.

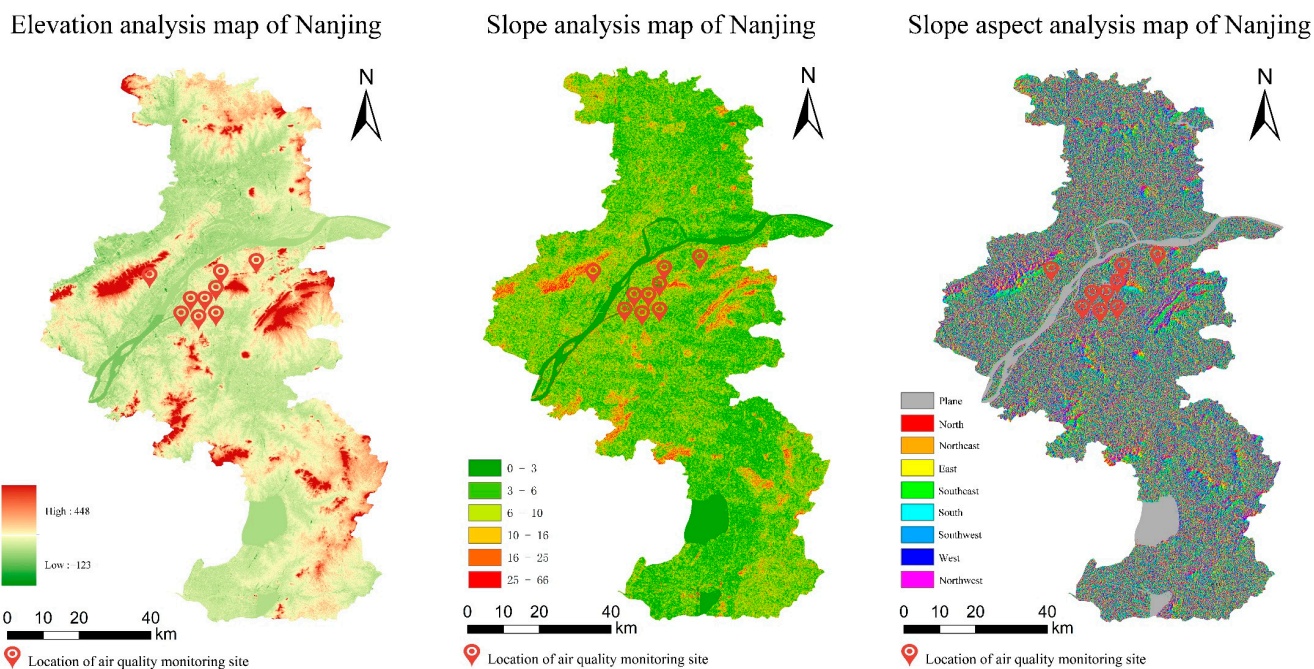


Figure 2. The analysis of elevation, slope, and slope aspects in Nanjing.

2.3.2. Spatiotemporal Distributions and Concentrations of Air Pollutants

The data for the six air pollutants in different areas underwent a screening process to eliminate any missing, abnormal, or invalid entries. The data corresponding to the air pollutants at the nine monitoring points for each year were then classified and screened

to determine the concentrations of six specific pollutants: SO₂, NO₂, CO, O₃, PM_{2.5}, and PM₁₀. Mean annual values of pollutant concentrations at each monitoring point were subsequently calculated. The air pollution data were also compared to the Chinese national concentration limits for key ambient air pollutants (Table 2). For the purpose of analysis, data from three years (2013, 2017, and 2021) within the 2013–2021 timeframe were chosen and averaged. To obtain spatial distribution maps illustrating the levels of atmospheric pollutants at each monitoring point in the Nanjing region, the Kriging method was employed for the interpolation of annual mean concentration values. The application of the Kriging interpolation method facilitated the creation of spatial distribution maps depicting the levels of air pollutants at each monitoring point [42].

Table 2. Concentration limits for essential items of atmospheric pollutants.

Sequence Number	Pollutant	Average Times	Concentration Limits		Unit
			Level 1	Level 2	
1	Sulfur dioxide (SO ₂)	Annual average	20	60	μg/m ³
		24-h average	50	150	
		1-h average	150	500	
2	Nitrogen dioxide (NO ₂)	Annual average	40	40	μg/m ³
		24-h average	80	80	
		1-h average	200	200	
3	Carbon monoxide (CO)	24-h average	4	4	mg/m ³
		1-h average	10	10	
4	Ozone (O ₃)	Daily maximum	100	160	μg/m ³
		8-h average	160	200	
		1-h average	160	200	
5	Particulate matter (PM ₁₀)	Annual average	40	70	μg/m ³
		24-h average	50	150	
6	Particulate matter (PM _{2.5})	Annual average	15	35	μg/m ³
		24-h average	35	75	

2.3.3. Heatmap Generation

This study aims to examine the correlations between air pollutants, socio-economic indicators, and NDVI in Nanjing from 2013 to 2021. To assess the socio-economic indicators, we selected six representative variables based on the Nanjing Statistical Yearbook. These indicators include gross industrial product, the first industry, the secondary industry, the third industry, GDP per capita, and urban population density [43,44]. For the generation of the heatmap, we utilized Origin 2022 software.

2.3.4. Correlation Analysis

In order to examine the relationships between air pollutants, minimum, average, and maximum NDVI values in various buffer zones (500 m, 1 km, and 2 km) at the nine monitoring sites and socio-economic indicators in Nanjing, a correlation analysis was conducted. This analysis aimed to determine the strength and direction of the linear relationships between the variables. The correlation coefficient (R^2) was utilized, ranging from -1 to 1 . The proximity of the r value to 1 or -1 indicates a more substantial positive or negative correlation between the variables, respectively [45].

3. Results and Discussion

3.1. Spatial Characteristics of Air Pollutants in Nanjing

The average daily concentrations of the six air pollutants in Nanjing between 2013 and 2021 were examined, and their spatial distribution and patterns in each area are depicted in Figure 3. Among the nine monitoring points, Ruijin Road exhibited the highest levels

of SO_2 , NO_2 , CO , and $\text{PM}_{2.5}$, with maximum concentrations of $44 \mu\text{g}/\text{m}^3$ for SO_2 and $116 \mu\text{g}/\text{m}^3$ for NO_2 . The upper range of SO_2 , NO_2 , CO , and $\text{PM}_{2.5}$ concentrations fell within the interval of 23, 62, 1.3, and $68 \mu\text{g}/\text{m}^3$, respectively. Based on the “Ambient Air Quality Standards” issued by the Ministry of Environmental Protection of the People’s Republic of China, all nine monitoring points, including residential, mixed-use, cultural, industrial, and rural areas, were classified as “Class 2 areas.” The daily mean concentration limits for SO_2 and NO_2 in these areas are 150 and $80 \mu\text{g}/\text{m}^3$, respectively. While the mean daily concentration of SO_2 fell within the regulatory range, the concentration of NO_2 significantly exceeded the standard limit. Although the concentrations of certain air pollutants remained relatively stable within specific intervals at the monitoring points, their magnitudes of change were notably high at certain times. For instance, the maximum $\text{PM}_{2.5}$ concentration at each monitoring point increased by over three times the box model value, primarily between 2013 and 2015. The concentrations of SO_2 and NO_2 , as the critical traffic-related pollutant gases, also demonstrated significant fluctuations exceeding 200% at three monitoring points, namely Ruijin Road, Shanxi Road, and Zhonghuamen, with the fluctuation primarily occurring between 2013 and 2016. This analysis confirms that the spatiotemporal characteristics of different monitoring points influence the concentrations of air pollutants. Among the monitoring points, Maigaoqiao displayed the lowest O_3 concentration; however, the steady-state box model values ranged between 47 and $57.7 \mu\text{g}/\text{m}^3$, with a peak value of $176 \mu\text{g}/\text{m}^3$, indicating an increase of over 300%. The O_3 concentration did not exhibit significant variations across the nine points.

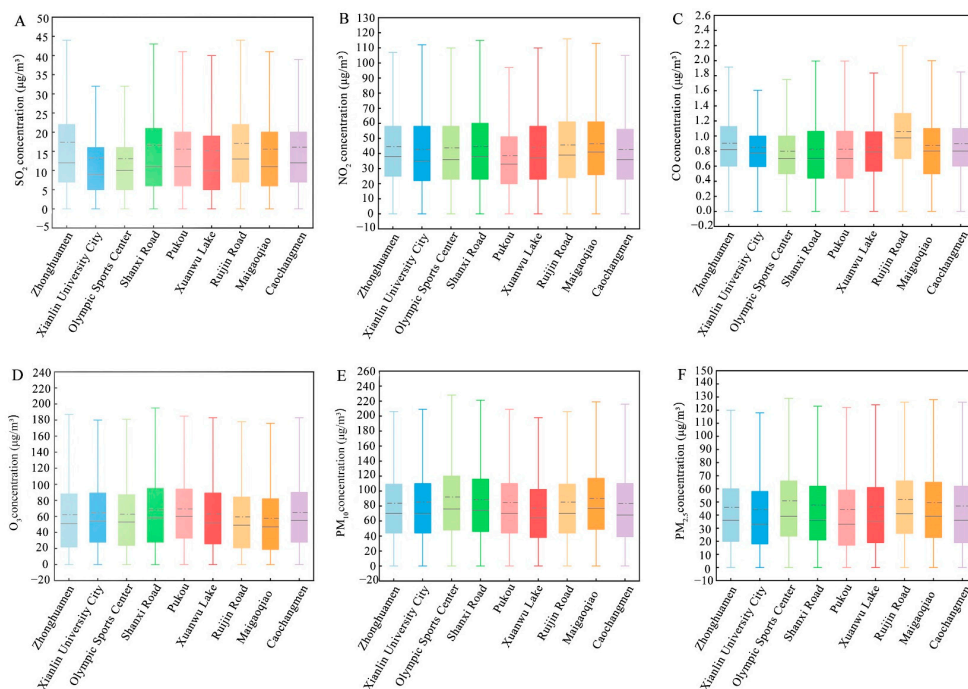


Figure 3. The spatiotemporal variations in the concentration of air pollutants in Nanjing (from 2013 to 2021). (A) spatiotemporal variations in SO_2 concentration; (B) spatiotemporal variations in NO_2 concentration; (C) spatiotemporal variations in CO concentration; (D) spatiotemporal variations in O_3 concentration; (E) spatiotemporal variations in PM_{10} concentration; (F) spatiotemporal variations in $\text{PM}_{2.5}$ concentration.

Spatial distribution maps were generated to depict the locations of the different districts where the monitoring points were situated (Figure 4). Between 2013 and 2021, all six pollutant concentrations exhibited a downward trend. The highest concentrations of CO and NO_2 at the monitoring points decreased from $1.17 \text{ mg}/\text{m}^3$ and $54.13 \mu\text{g}/\text{m}^3$ to $0.92 \text{ mg}/\text{m}^3$ and $38.49 \mu\text{g}/\text{m}^3$, respectively. The concentration of O_3 initially increased and then decreased, reaching a peak value of $77.38 \mu\text{g}/\text{m}^3$ in 2017 before decreasing

to $67.72 \mu\text{g}/\text{m}^3$ in 2021. Notably, the PM_{10} concentration exhibited the most significant reduction, declining from a maximum value of $103.77 \mu\text{g}/\text{m}^3$ in 2013 to $76.77 \mu\text{g}/\text{m}^3$ in 2021. The highest concentration of SO_2 decreased from $38.24 \mu\text{g}/\text{m}^3$ in 2013 to $7.54 \mu\text{g}/\text{m}^3$ in 2021, while the $\text{PM}_{2.5}$ concentration similarly decreased from $74.85 \mu\text{g}/\text{m}^3$ to $33.24 \mu\text{g}/\text{m}^3$. Overall, Pukou District and Qixia District displayed the best ambient air quality, while Xuanwu District and Gulou District had relatively poorer air quality. Significantly, the concentration of environmental air pollutants gradually decreased from the center to the surrounding areas of the central urban region.



Figure 4. Trend in the annual average concentration distribution of pollutants in Nanjing in 2013, 2017, and 2021. (A) average annual concentration of SO_2 in 2013; (B) average annual concentration of NO_2 in 2013; (C) average annual concentration of CO in 2013; (D) average annual concentration of O_3 in 2013; (E) average annual concentration of PM_{10} in 2013; (F) average annual concentration of $\text{PM}_{2.5}$ in 2013; (G) average annual concentration of SO_2 in 2017; (H) average annual concentration of NO_2 in 2017; (I) average annual concentration of CO in 2017; (J) average annual concentration of O_3 in 2017; (K) average annual concentration of PM_{10} in 2017; (L) average annual concentration of $\text{PM}_{2.5}$ in 2017; (M) average annual concentration of SO_2 in 2021; (N) average annual concentration of NO_2 in 2021; (O) average annual concentration of CO in 2021; (P) average annual concentration of O_3 in 2021; (Q) average annual concentration of PM_{10} in 2021; (R) average annual concentration of $\text{PM}_{2.5}$ in 2021.

In this study, nine monitoring sites were carefully selected to ensure accurate measurements of pollutants across different spatial scales [46,47]. The results revealed variations in the concentrations of the six air pollutants among these sites in Nanjing. Ruijin Road and Shanxi Road stood out as locations with notably higher pollutant levels. In contrast, recreational areas like Xuanwu Lake showcased relatively low pollutant concentrations. As expected, monitoring sites near roads, densely populated areas, and industrial zones exhibited higher pollutant levels compared to standard values due to exhaust and industrial emissions. Conversely, areas with well-designed landscape patterns demonstrated lower pollutant concentrations. The monitoring sites located near roads and densely populated

urban areas showed more pronounced intensity in pollutant concentration and sensitivity. These findings align with Zhao, Y.Y. et al., who conducted a similar analysis on the influence of socio-economic activities on air pollutants [48]. Previous studies have also reported significant outcomes by employing a radial buffer range of 3 km to study air pollutants, such as PM_{2.5}, and assess vegetation patterns and urban green spaces [49].

3.2. Temporal Variation Patterns of Air Pollutants in Nanjing

Based on long-term meteorological data, the study period was divided into winter (December–February) and summer (June–August) seasons. The seasonal fluctuations in NO₂, CO, SO₂, PM_{2.5}, and PM₁₀ (except for O₃) between 2013 and 2021 exhibited a consistent pattern, with higher concentrations observed in winter and lower concentrations in summer (Figure 5). Throughout the entire period, the mean concentration of SO₂ was highest in the winter of 2013, peaking at 44.25 µg/m³. However, by 2021, both the mean summer and winter concentrations of SO₂ were low and similar, measuring 5.4 and 5.9 µg/m³, respectively. The concentration of SO₂ gradually decreased over time during both winter and summer seasons. The mean concentration of NO₂ in summer exhibited a clear downward trend, reaching 21.05 µg/m³ in 2021, which was below the secondary emission standard for NO₂. In contrast, the average concentration of NO₂ in winter was 66.95 µg/m³ in 2013 and remained relatively stable at around 54 µg/m³ until 2021. The summer concentration of CO exhibited a gradual decline with slight fluctuations ranging from 0.6 to 0.9 mg/m³. In contrast to other air pollutants, the variation in the concentration of O₃ differed, with lower levels observed in winter and higher levels in summer. Starting from 2013, the concentration of O₃ continuously increased, reaching its peak of 263 µg/m³ in the summer of 2019. Both PM_{2.5} and PM₁₀ showed similar variations, with their highest concentrations occurring in winter each year. In the winter of 2013, the maximum values of PM_{2.5} and PM₁₀ were recorded as 30 and 474 µg/m³, respectively. Over the course of the study, both PM_{2.5} and PM₁₀ concentrations decreased in both winter and summer seasons.

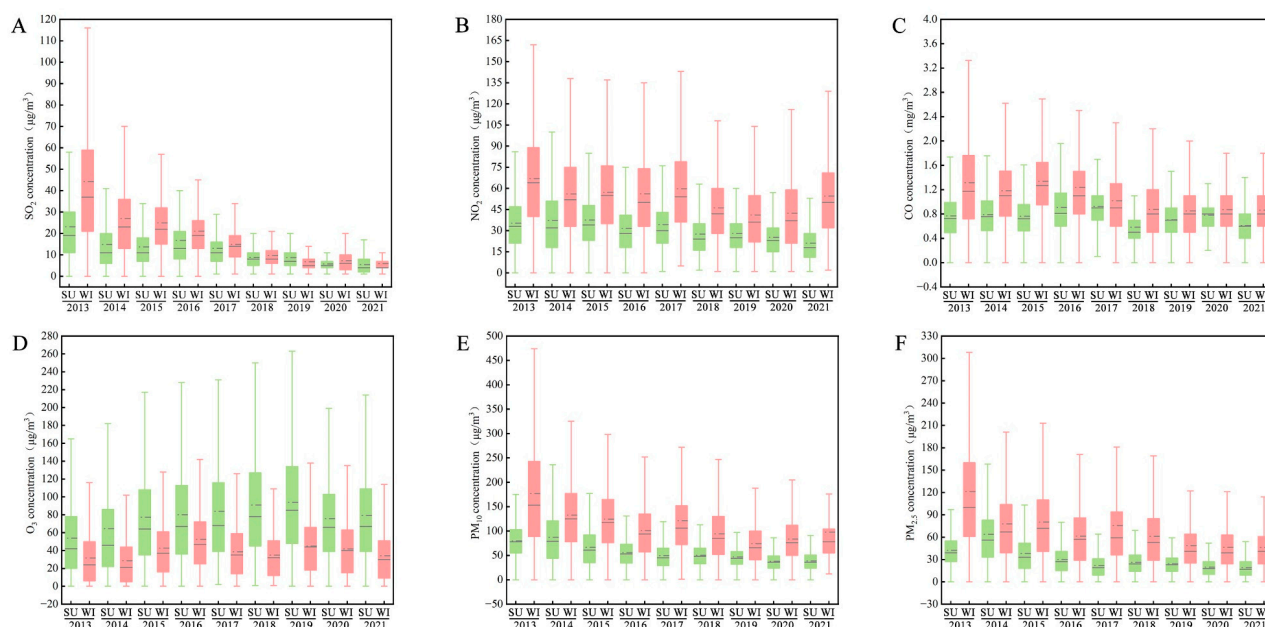


Figure 5. Changes in seasonal average concentrations of various pollutants from 2013 to 2021. (A) changes in seasonal average concentrations of SO₂; (B) changes in seasonal average concentrations of NO₂; (C) changes in seasonal average concentrations of CO; (D) changes in seasonal average concentrations of O₃; (E) changes in seasonal average concentrations of PM₁₀; (F) changes in seasonal average concentrations of PM_{2.5}.

The study examined the average concentration of seasonal pollutants and determined that in summer, the concentrations of PM_{2.5}, SO₂, NO₂, CO, and PM₁₀ were lower compared

to winter. These results align with a previous study by Liu et al., which also found a notable negative correlation between air temperature and the concentrations of PM_{2.5}, SO₂, NO₂, and other pollutants in Luoyang [50]. In this study, it was observed that seasonal summer winds exhibited greater intensity and frequency compared to winter winds. Similar findings were reported by Tao et al. [51], who also noted that during winter, air pollutant dispersion was not apparent in the absence of consistent wind direction, resulting in higher pollutant accumulation. Analyzing the yearly time dimension, a gradual decrease in the concentrations of PM_{2.5}, SO₂, NO₂, CO, and PM₁₀ was observed. Notably, the decrease in SO₂ concentration was the most remarkable, with a reduction of approximately 75% between 2013 and 2021. The remaining four pollutants displayed less fluctuation but exhibited an overall decreasing trend over time. Since the occurrence of a rare haze event in East China in 2013, Nanjing has taken swift measures towards industrial restructuring and accelerated economic transformation [52]. The Nanjing Municipal Government has implemented a series of progressive environmental protection policies and measures, such as the “13th Five-Year Plan for Ecological Environment Protection in Nanjing” (2016) and the “Nanjing Environmental Protection Regulations” (2017). As a result, the quality of the ecological environment in Nanjing has consistently improved over the years [53]. However, unlike other air pollutants, concentrations of O₃ increased. O₃ was the only pollutant with higher concentrations in summer compared to winter. These findings align with the studies conducted by Xu et al. in Chongqing and Shao et al. in Jiazhangkou [54,55]. The higher concentrations of O₃ in summer can be attributed to the elevated temperatures and intense solar radiation, which provide favorable conditions for its formation. Overall, the concentrations of air pollutants were higher in winter than in summer, primarily due to the drier climate and lower wind speeds during winter, as well as human-induced factors like vehicle exhaust emissions and heating [56]. The overall efficiency of vegetation in removing pollutants was also lower during winter compared to summer.

3.3. Analysis of NDVI, GVI, and RVI Indexes in Nanjing

3.3.1. NDVI Variation

Figure 6 presents the spatial pattern of NDVI values in Nanjing from 2013 to 2021. The pattern observed was as follows: the north region exhibited the highest values, followed by the west, east, and south regions. In terms of seasonal variation, the overall variation was lower during winter compared to summer. The maximum NDVI value ranged between 0.79 and 1, with the lowest value recorded in 2013. Conversely, the minimum NDVI value ranged between −1 and −0.33, with −1 being the lowest except for the winter of 2013 (−0.41) and the summer of 2020 (−0.33). Specifically, the northwestern part of Nanjing, characterized by forest land, displayed high NDVI values. In the eastern area, where farmland predominates, the NDVI values were higher during the summer and autumn. The central area along the river, primarily composed of built-up land, exhibited a low NDVI value, indicating poor vegetation cover and a limited ability to reduce surface dust. Finally, the southwestern area, which mainly comprises water bodies, notably Shijiu Lake, also displayed a low NDVI value.

In this study, variations in land use classes were found to correspond to variations in vegetation cover. The Xuanwu Lake area, designed and managed as a recreational site, exhibited high NDVI values and relatively low concentrations of air pollutants. The spatial analysis of NDVI displayed lower values in areas with limited vegetation cover, such as lakes, farmlands, and densely built-up areas. As depicted in Figure 7, there was no significant disparity in NDVI between summer and winter. Zheng et al. [57] discovered that climate factors, including precipitation and temperature, influence the vegetation index in the China–Pakistan Corridor, with the correlation between precipitation and temperature being more robust than that of temperature alone. The relatively minor variance in NDVI between summer and winter may be attributed to insufficient rainfall in recent years or potentially influenced by other factors like human activities.

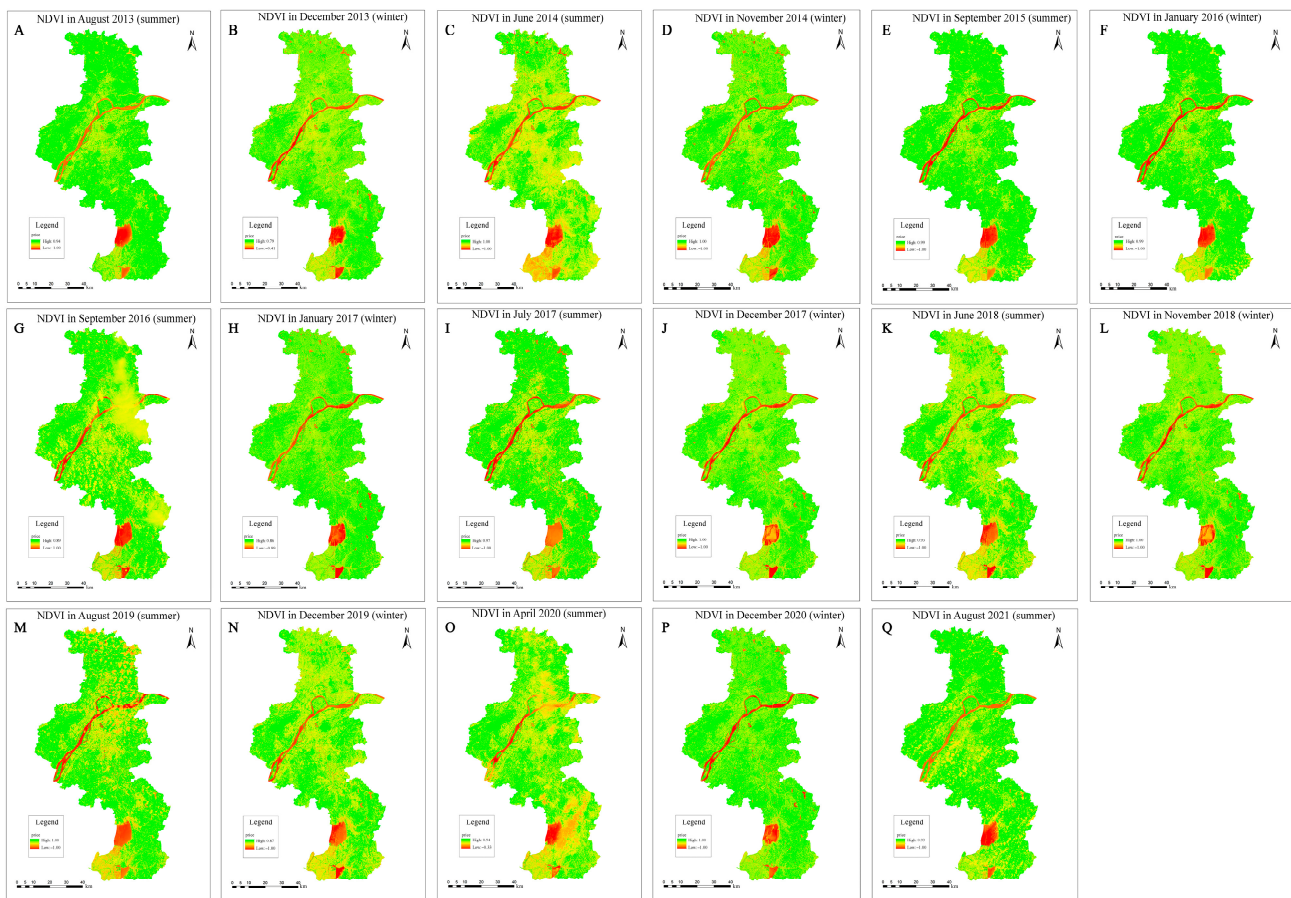


Figure 6. Comparison of seasonal NDVI data between summer and winter from 2013 to 2021. (A) NDVI in August 2013; (B) NDVI in December 2013; (C) NDVI in June 2014; (D) NDVI in November 2014; (E) NDVI in September 2015; (F) NDVI in January 2016; (G) NDVI in September 2016; (H) NDVI in January 2017; (I) NDVI in July 2017; (J) NDVI in December 2017; (K) NDVI in June 2018; (L) NDVI in November 2018; (M) NDVI in August 2019; (N) NDVI in December 2019; (O) NDVI in April 2020; (P) NDVI in December 2020; (Q) NDVI in August 2021.

3.3.2. RVI Variation

Figure 7 illustrates that the RVI values attained their peak in the northern part of the city and recorded their lowest values in the central region. Regarding seasonality, the RVI values were lower in winter compared to summer. The summer of 2014 saw the highest RVI value of 255, marking an 85% increase in comparison to the RVI value recorded during the winter of the same year. From the summer of 2013 to the summer of 2021, there was a notable decrease in the highest RVI value, declining from 36.312 to 23.501, reflecting a 22% decrease. In contrast to summer, the maximum RVI value witnessed an 88% increase from the winter of 2013 to the winter of 2020, rising from 7.961 to 126. Notably, the winter of 2020 recorded the highest RVI value among all winters within the nine-year period. In general, the index values exhibited substantial variation, aside from the relatively consistent RVI values observed in the northwest and southeast regions of the city. Furthermore, the vegetation index values were lower in the area north of the Yangtze River compared to its southern counterpart. Overall, the RVI value was significantly lower during winter than during summer.

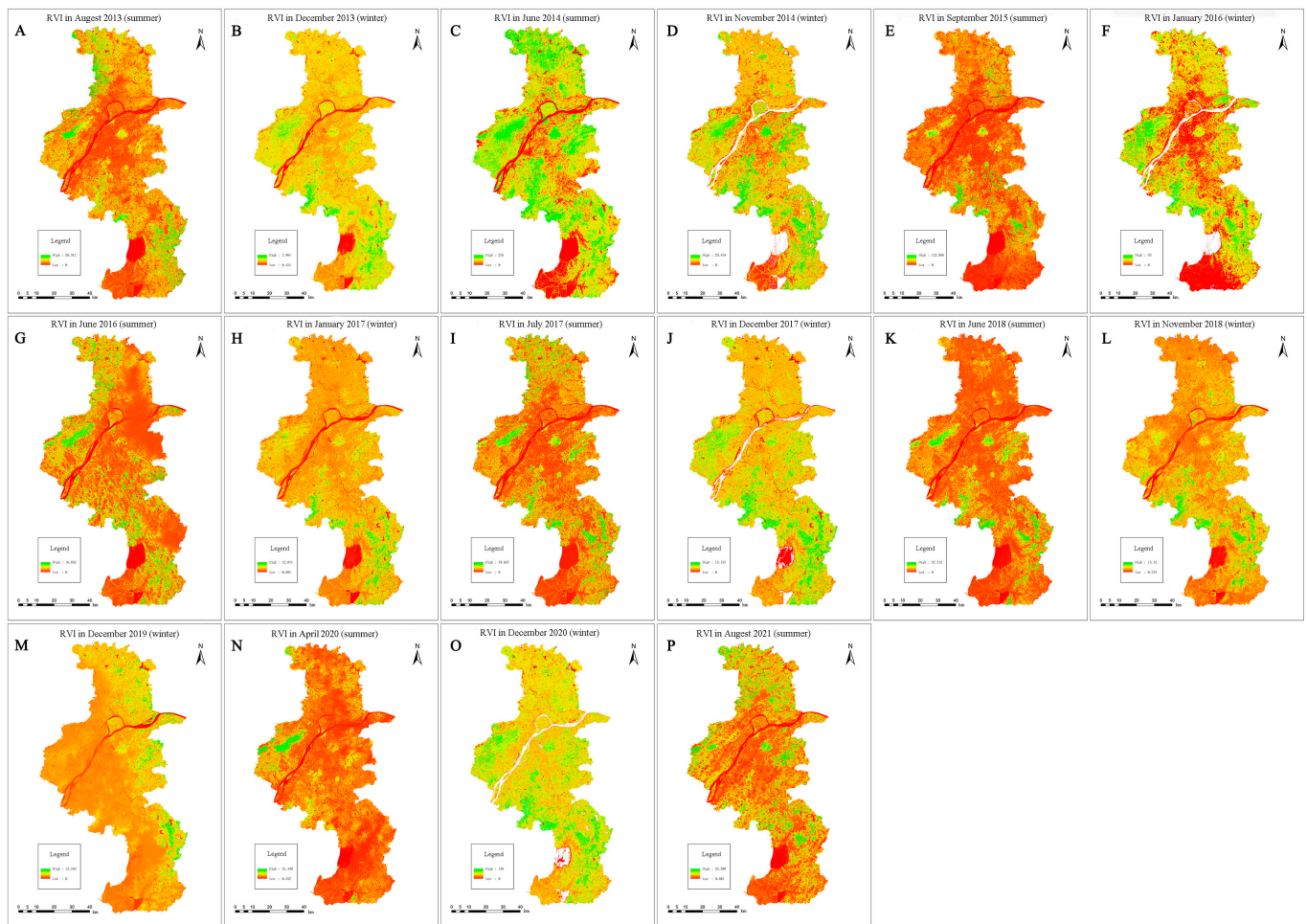


Figure 7. Comparison of summer and winter RVI data from 2013 to 2021. (A) RVI in August 2013; (B) RVI in December 2013; (C) RVI in June 2014; (D) RVI in November 2014; (E) RVI in September 2015; (F) RVI in January 2016; (G) RVI in June 2016; (H) RVI in January 2017; (I) RVI in July 2017; (J) RVI in December 2017; (K) RVI in June 2018; (L) RVI in November 2018; (M) RVI in December 2019; (N) RVI in April 2020; (O) RVI in December 2020; (P) RVI in August 2021.

3.3.3. GVI Variation

The GVI serves as a means to assess the level of plant greenness. As depicted in Figure 8, there was an overall upward trend in the GVI values over time, which exhibited a partial positive correlation with the seasonal variations observed in the RVI values. To illustrate, the RVI values for the summers of 2014, 2015, and 2019 exceeded the GVI values for the other summers, recording values of 255, 141, and 457, respectively. The maximum GVI values for the remaining summers fell within the range of 11.405 to 35.549. In contrast, the GVI values during winter demonstrated an increasing pattern over time. The highest GVI value was observed in the winter of 2013, reaching 7.388, while in the winter of 2020, it reached 24, presenting a 53% increase. Comparatively, the GVI values were higher during summer than in winter, and the central area exhibited lower GVI values in contrast to the surrounding areas with higher values.

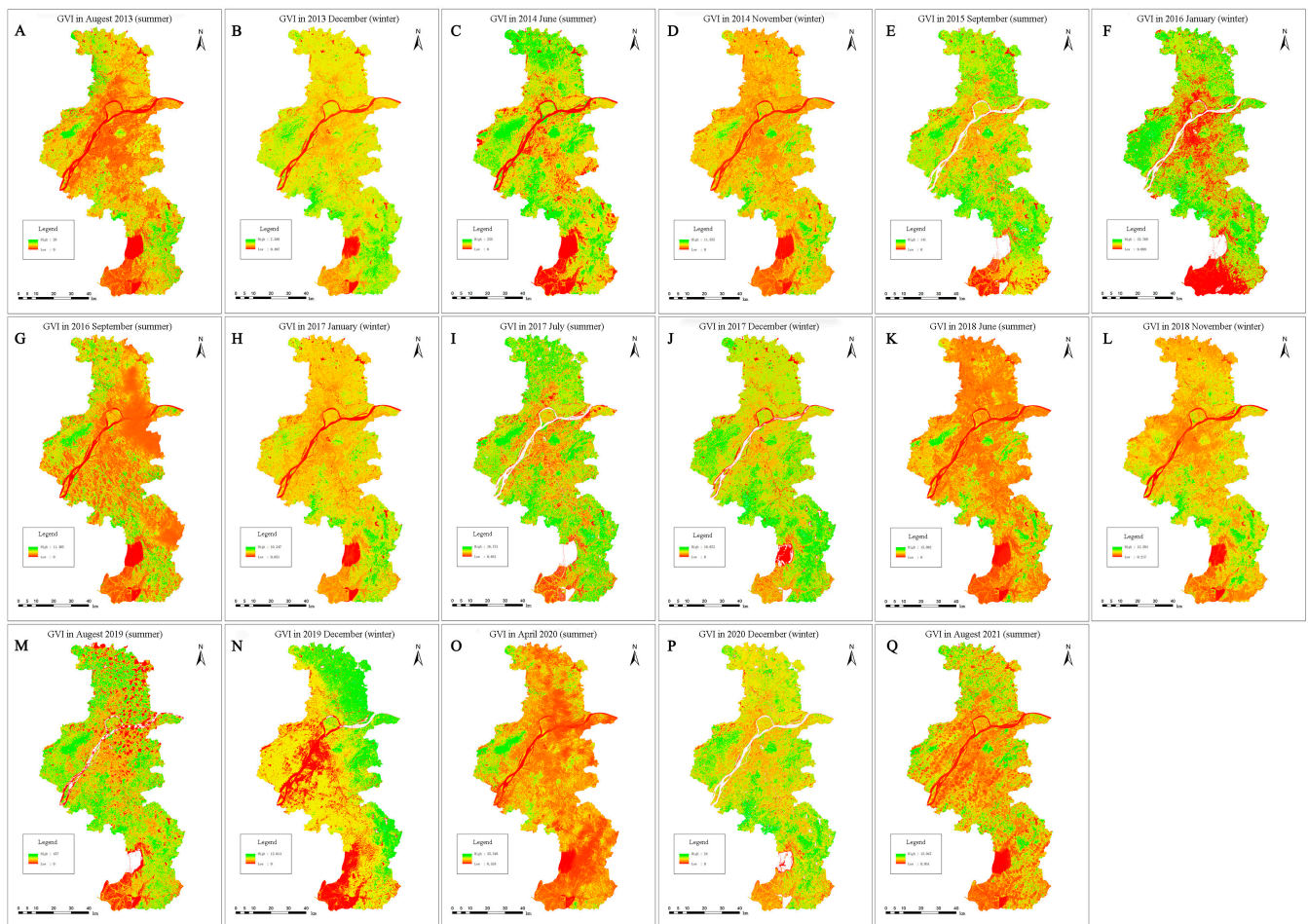


Figure 8. Comparison of summer and winter GVI data from 2013 to 2021. (A) GVI in August 2013; (B) GVI in December 2013; (C) GVI in June 2014; (D) GVI in November 2014; (E) GVI in September 2015; (F) GVI in January 2016; (G) GVI in September 2016; (H) GVI in January 2017; (I) GVI in July 2017; (J) GVI in December 2017; (K) GVI in June 2018; (L) GVI in November 2018; (M) GVI in August 2019; (N) GVI in December 2019; (O) GVI in April 2020; (P) GVI in December 2020; (Q) GVI in August 2021.

3.4. Effects of Vegetation Indices on Air Pollutants

Given the intricate spatiotemporal interactions between urban landscape patterns and atmospheric effects [58], urban planning must be formulated and implemented while considering the interconnectedness of all ecosystem components. Similarly, the complexity lies in the multitude of factors and their interactions within the urban landscape, influencing its capacity to mitigate air pollutants. The vegetation index serves as a means to assess the association between vegetation cover and plant growth vitality, with consideration for multiple aspects related to air pollution. Through data processing with ArcGIS 10.8 software, it was observed that external factors exerted a more substantial influence on the spatial distributions of GVI. RVI demonstrated a weaker sensitivity to areas with limited vegetation cover. Conversely, NDVI exhibited a closer relationship with vegetation distribution and dynamics compared to the other indices. Consequently, this study focused on exploring the correlations between NDVI and air pollutants.

3.4.1. Correlation Analysis of NDVI and Air Pollutants

Based on the findings from the linear regression model, which was selected as the best fit for all three buffer zones and the six air pollutants (refer to Table 3), the relationships between NDVI and the minimum and average concentrations of the six pollutants were

characterized by relatively low R^2 values. However, within the 500 m distance range, the maximum NDVI values demonstrated stronger correlations with the concentrations of SO_2 , PM_{10} , and $\text{PM}_{2.5}$, with respective R^2 values of 0.6280, 0.6350, and 0.6881. These findings suggest that these three pollutants exhibit a strong alignment with the NDVI values. In the 1 km distance range, while the correlation between NDVI and CO concentration was low, the R^2 values for the remaining five pollutants were all above 0.5. Notably, the correlation between $\text{PM}_{2.5}$ and NDVI exceeded 0.8. Furthermore, in the 2 km buffer zone, the R^2 values between each air pollutant and NDVI were consistent with those observed in the 1 km range. Overall, the expansion of the buffer zone resulted in an increasing trend in both NDVI values and the fitting results for the six pollutants.

Table 3. R^2 values of the best-fit linear regression models between NDVI and six air pollutants at various radii.

Pollutant	NDVI-500 m			NDVI-1 km			NDVI-2 km		
	Minimum Value	Average Value	Maximum Value	Minimum Value	Average Value	Maximum Value	Minimum Value	Average Value	Maximum Value
SO_2	0.017	0.0751	0.628	0.0038	0.1187	0.7404	0.0018	0.126	0.8409
NO_2	0.046	0.0683	0.4695	0.0175	0.1113	0.5241	0.0185	0.1601	0.6269
CO	0.0787	0.0462	0.2008	0.0775	0.0713	0.2652	0.1306	0.136	0.3514
O_3	3.45×10^{-4}	0.1137	0.4557	0.0307	0.1445	0.5905	0.0266	0.1268	0.5206
PM_{10}	9.16×10^{-5}	0.0508	0.635	0.006	0.068	0.729	0.0042	0.08	0.8365
$\text{PM}_{2.5}$	5.55×10^{-6}	0.0761	0.6881	0.0067	0.1036	0.8086	0.0016	0.1119	0.8627

3.4.2. Effects of NDVI on Air Pollutants

Within the range of 500 m to 2 km from the monitoring sites, significant correlations between NDVI and SO_2 , $\text{PM}_{2.5}$, and PM_{10} were observed. Given the relatively stable relationships between NDVI and each air pollutant in the 2 km range, our analysis focused on this specific range. As depicted in Figure 9, a decreasing trend in SO_2 , NO_2 , CO, PM_{10} , and $\text{PM}_{2.5}$ concentrations, particularly the latter two, was evident as NDVI levels increased. This pattern can be attributed to the implementation of the “Air Pollution Prevention and Control Action Plan,” which has contributed to reducing air pollutants, notably $\text{PM}_{2.5}$, in Nanjing. Figure 10 displays small statistical dispersions for $\text{PM}_{2.5}$, PM_{10} , and NDVI, with respective R^2 values of 0.83 and 0.86. Consistent with Zang et al. (2021), who explored Henan Province, $\text{PM}_{2.5}$ and PM_{10} demonstrated significant negative correlations with NDVI and precipitation [59]. In our study, the relationship between CO and NDVI exhibited a large statistical dispersion, with an R^2 value of only 0.33. This discrepancy may be attributed to the lower concentrations of CO itself, making it more susceptible to other factors not extensively examined in this study, such as land management practices [60] and dust emissions [61]. Notably, among all pollutants, O_3 displayed a positive correlation with NDVI ($R^2 = 0.5$). This finding aligns with the results reported by Miao et al. [62]. However, their study indicates that the relationship between O_3 pollution levels and vegetation growth was insignificant. Distinct from other pollutants, the increased concentrations of O_3 noted in our study emphasize its potential as a primary factor influencing air quality.

3.5. Correlation Analysis of NDVI, Air Pollutants and Socio-Economic Data

Currently, numerous scholars employ NDVI values as indicators to assess vegetation growth, development, environmental and ecological changes, as well as to analyze their correlation with atmospheric pollutants and socio-economic factors [63–65]. In light of this, the present study aims to delve deeper into the correlation between NDVI values and atmospheric pollutants alongside local socio-economic data, specifically in the context of Nanjing.

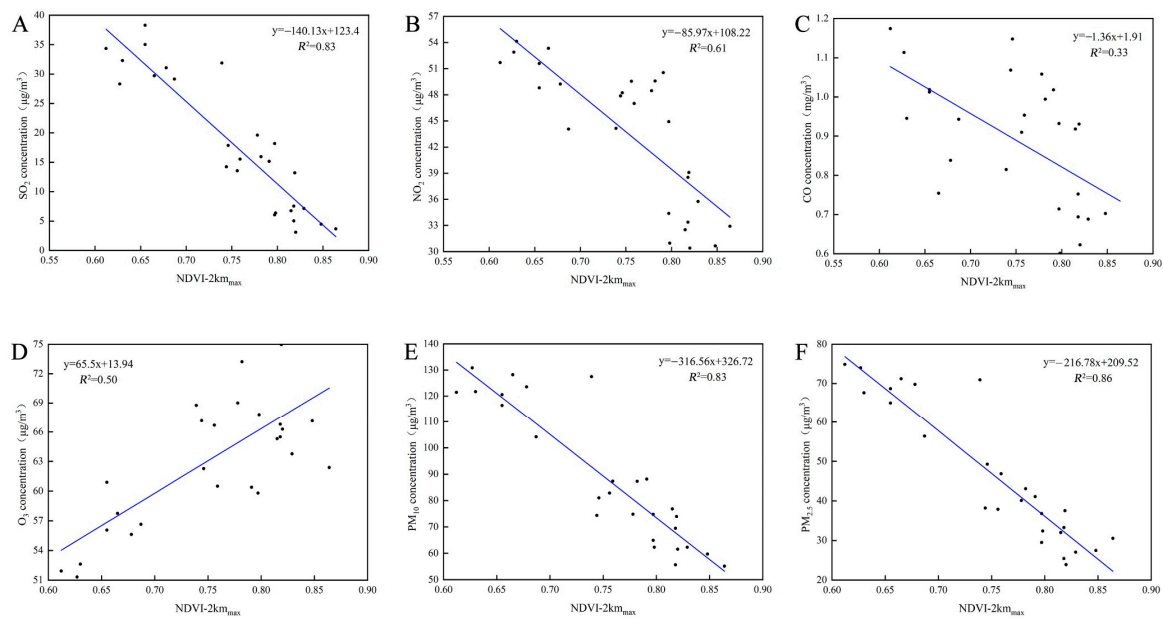


Figure 9. The best-fit linear regression models between the six pollutants and NDVI (2 km_{max} values). (A) SO₂ concentration and NDVI (2 km_{max} values); (B) NO₂ concentration and NDVI (2 km_{max} values); (C) CO concentration and NDVI (2 km_{max} values); (D) O₃ concentration and NDVI (2 km_{max} values); (E) PM₁₀ concentration and NDVI (2 km_{max} values); (F) PM_{2.5} concentration and NDVI (2 km_{max} values).

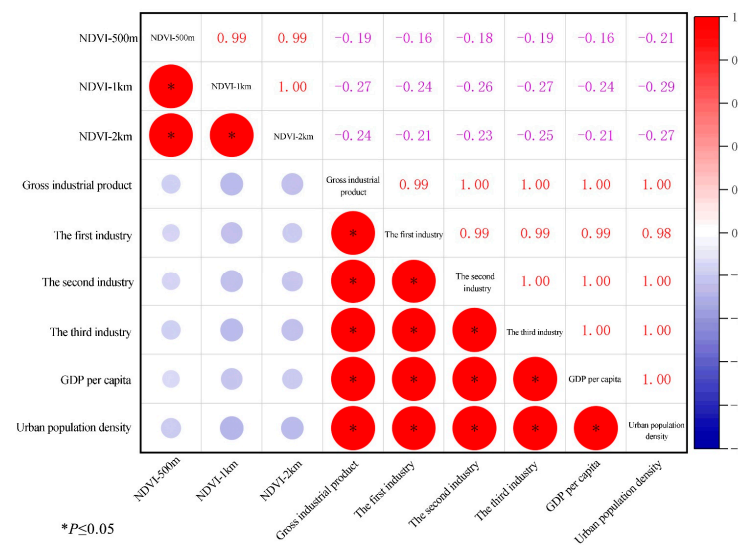


Figure 10. Heatmap of the correlations between NDVI and socio-economic data.

3.5.1. Heatmap Analysis of Correlation between NDVI and Socio-Economic Data

The socioeconomic state of Nanjing was assessed using indicators such as Industrial Gross Value Added, population, GDP, and urban population density. The relationships between NDVI and these socioeconomic indicators, as well as air pollution data, were analyzed through best-fit linear regression models. As depicted in Figure 10, NDVI values within all three buffer zones displayed negative correlations with the socioeconomic indicators, although these correlations were not statistically significant. Notably, a significant correlation between NDVI and economic growth was observed within the 1 km buffer zone, while urban population density exhibited the strongest correlation with NDVI. In essence, increased urban population density and economic growth had a detrimental impact on vegetation.

3.5.2. Heatmap Analysis of Correlation between Air Pollutants and Socio-Economic Data

Figure 11 demonstrates a highly significant positive correlation between O₃ concentration and socioeconomic indicators. Both R² values exceed 0.8, with the primary industry value surpassing 0.9. This indicates that O₃ concentrations increase alongside rapid economic growth. Conversely, the other five pollutants exhibit negative correlations with economic growth. Correlations between SO₂, NO₂, PM₁₀, and PM_{2.5} concentrations and the socioeconomic indicators all exceed 0.8, with some surpassing 0.9. However, the correlation between CO concentrations and socioeconomic indicators is only around 0.5. Overall, aside from O₃ concentration, negative correlations were observed between the concentrations of other pollutants and social and economic indicators. Additionally, gross domestic product and population density in Nanjing are positively correlated with O₃ concentrations. The release of nitrogen oxides and volatile organic compounds, combined with sunlight, contributes to the production of O₃ and its increased atmospheric concentration. This implies that as industrialization levels rise and energy consumption demands increase, emissions of O₃ precursor substances from industrial production also increase. However, the concentrations of the other five pollutants have exhibited a decreasing trend over the study period. This trend can be attributed to the implementation of various environmental protection measures in Nanjing, including the “Nanjing Ecological Civilization Construction Plan (2013–2020),” which has positively contributed to the improved environmental quality of the city. In conclusion, the implementation of environmentally preventive and mitigative measures, combined with ongoing economic growth, greatly promotes the harmonious coexistence and development of both the economy and the urban environment.

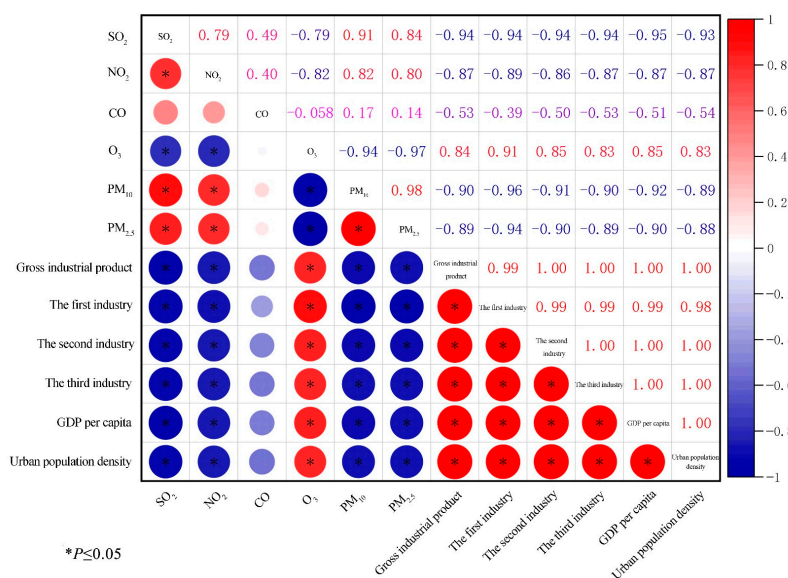


Figure 11. Heatmap of the correlation between the six pollutants and the socio-economic data.

4. Conclusions

Based on data processing and subsequent discussion of the results, the following conclusions have been drawn. Firstly, the spatial distribution of the six air pollutants in Nanjing showcases a gradual decrease from the city center to peripheral areas. Overall, the main urban area experiences the poorest air quality, while the Pukou and Qixia Districts exhibit the best air quality. Secondly, there has been a moderate decline in air quality in Nanjing from 2013 to 2021, particularly for PM_{2.5} and PM₁₀. The temporal pattern of the concentrations of SO₂, NO₂, CO, PM_{2.5}, and PM₁₀ indicates higher levels during winter compared to summer. Notably, increasing O₃ concentrations signify its emergence as a potential future contributor to air pollution. Moreover, through correlation analysis of the three vegetation indices and air pollutants, a strong alignment is observed between the spatial distributions of vegetation indices and air pollutants. A favorable linear relationship

exists between NDVI and all air pollutants except for CO. As NDVI values increase, the concentrations of the five pollutants decrease, whereas CO concentration remains unaffected by NDVI. Lastly, NDVI demonstrates a weak negative correlation with socioeconomic factors in general. As population density and economic levels continue to rise, vegetation coverage experiences a negative impact. The air pollutants exhibit a robust correlation with socioeconomic factors, primarily influenced by industrial production and human-induced disturbances. In the context of Nanjing's future urban development, it is imperative to persist in the execution of existing ecological conservation projects, bolster urban green space planning, and promote a gradual augmentation in vegetation coverage. Additionally, harnessing cutting-edge achievements in modern science and technology, optimizing industrial structures, and facilitating the transition and upgrading of traditional industries toward sustainable, environmentally-conscious practices are of paramount importance. These findings hold significant implications for enhancing regional air quality and provide a scientific foundation, along with technical support, for subsequent prevention, control, and management of air pollution in Nanjing.

Author Contributions: Conceptualization, Q.S.; software, H.Z.; formal analysis, Y.J., C.Z. and H.Z.; data curation, Y.J.; writing—original draft, Y.J. and C.Z.; writing—review & editing, Q.S.; supervision, Z.Z.; project administration, Z.Z.; funding acquisition, Q.S. and Z.Z. All authors have read and agreed to the published version of the manuscript.

Funding: This research was funded by the Ministry of Education Humanities and Social Sciences Research “Study on the new mechanism of urban green space ecological benefit Measurement and high-quality collaborative development: A case study of Nanjing Metropolitan Area”: grant number 21YJCZH131; Young elite scientist sponsorship program by cast in China Association for Science and Technology: grant number YESS20220054; Social Science Foundation Project of Jiangsu Province: grant number 21GLC002; National Natural Science Foundation of China: grant number 32101582; Natural Science Foundation of Jiangsu Province of China: grant number BK20210613; The Natural Science Foundation of the Jiangsu Higher Education Institutions of China: grant number 21KJB220008; The National Natural Science Foundation of China: grant number 32071832; “Qing Lan Project” in Jiangsu Province of China: grant number None. And The APC was funded by Zunling Zhu.

Data Availability Statement: Not applicable.

Acknowledgments: We express our sincere gratitude to Weizheng Li from the Advanced Analysis and Testing Center at Nanjing Forestry University and Ruizhen Yang from Nanjing Sky Hunt Data Technology Co., Ltd. for their invaluable assistance in data processing.

Conflicts of Interest: The authors declare no conflict of interest.

References

1. Maji, K.J.; Li, V.O.K.; Lam, J.C.K. Effects of China's current Air Pollution Prevention and Control Action Plan on air pollution patterns, health risks and mortalities in Beijing 2014–2018. *Chemosphere* **2020**, *260*, 127572. [[CrossRef](#)] [[PubMed](#)]
2. Liu, H.M.; Fang, C.L.; Huang, J.J.; Zhu, X.D.; Zhou, Y.; Wang, Z.B.; Zhang, Q. The spatial-temporal characteristics and influencing factors of air pollution in the Beijing-Tianjin-Hebei urban agglomeration. *J. Geogr.* **2018**, *73*, 177–191.
3. Chen, L.L.; Wang, H.; Wang, Z.W.; Dong, Z.M. Estimating the mortality attributable to indoor exposure to particulate matter of outdoor origin in mainland China. *Sci. Total Environ.* **2023**, *872*, 162286. [[CrossRef](#)] [[PubMed](#)]
4. Du, J.; Song, P.C.; Long, P.; Huang, Q.; Qiao, J.X. Characteristics and correlation analysis of atmospheric pollutant concentration changes in Mianyang. *J. Earth Environment* **2021**, *12*, 183–191+201.
5. Zhang, Y.J.; Cai, J.; Wang, S.X.; He, K.B.; Zheng, M. Review of receptor-based source apportionment research of fine particulate matter and its challenges in China. *Sci. Total Environ.* **2017**, *586*, 917–929. [[CrossRef](#)]
6. Wang, Y.G.; Ying, Q.; Hu, J.L.; Zhang, H.L. Spatial and temporal variations of six criteria air pollutants in 31 provincial capital cities in China during 2013–2014. *Environ. Int.* **2014**, *73*, 413–422. [[CrossRef](#)]
7. Wan, Q.; Chen, Z.; Wang, Y.; Feng, B. Multi-scale analysis of the spatial and temporal development of PM_{2.5} in the Yangtze River Economic Belt from 1998 to 2016. *Yangtze River Basin Resour. Environ.* **2019**, *28*, 2504–2512.
8. Banerjee, T.; Singh, S.B.; Srivastava, R.K. Development and performance evaluation of statistical models correlating air pollutants and meteorological variables at Pantnagar, India. *Atmos. Res.* **2011**, *99*, 505–517. [[CrossRef](#)]

9. Wang, J.H.; Zhao, T.B.; Ma, Y.X.; Ma, P.; Yang, S.M.; Wang, S. Characteristics of air pollution in Xi'an and their relationship with meteorological factors. *Environ. Chem.* **2015**, *34*, 386–387.
10. Jia, B.; Lu, J.W.; Li, X.; Wang, X. Trends of atmospheric pollutant concentrations and analysis of their influencing factors in Dianjiang, Chongqing. *Environ. Impact Assess.* **2016**, *38*, 78–81.
11. Hrishikesh, C.G.; Nagendra, S.M.S. Study of meteorological impact on air quality in a humid tropical urban area. *J. Earth Syst. Sci.* **2019**, *128*, 118. [[CrossRef](#)]
12. Cui, L.L.; Zhou, L.; Chen, X.D.; Zhang, X.Z.; Wang, Q.Q.; Wu, J.; Ding, Z. Characteristics of spatial and temporal variation in air pollutant concentrations in typical regions of Nanjing in the past 10 years. *Mod. Prev. Med.* **2013**, *40*, 3356–3360+3370.
13. Guo, Q.H.; Chen, K. Analysis of ambient air quality characteristics and variation in Nanjing. *J. Nanjing Univ. Inf. Eng. Nat. Sci. Ed.* **2022**, *14*, 294–303.
14. Yuan, X.; Huang, Z.J.; Lu, M.H.; Jia, G.L.; Duan, J.H.; Shen, J.; Zhong, Z.M.; Chen, D.H.; Zheng, J.Y. Seasonal evolution and cause analysis of ozone pollution in the Pearl River Delta based on observation and machine learning. *Acta Sci. Circumstantiae* **2023**, *43*, 214–225.
15. Ersin, Ö.Ö. The nonlinear relationship of environmental degradation and income for the 1870–2011 period in selected developed countries: The dynamic panel-star approach. *Procedia Econ. Financ.* **2016**, *38*, 318–339. [[CrossRef](#)]
16. Bildirici, M.; Ersin, Ö.Ö. Nexus between Industry 4.0 and environmental sustainability: A Fourier panel bootstrap cointegration and causality analysis. *J. Clean. Prod.* **2023**, *386*, 135786. [[CrossRef](#)]
17. Escobedo, S.; de Lasa, H. Photocatalysis for air treatment processes: Current technologies and future applications for the removal of organic pollutants and viruses. *Catalysts* **2020**, *10*, 966. [[CrossRef](#)]
18. Wang, Q.Y.; Enyoh, C.E.; Chowdhury, T.; Chowdhury, M.A.H. Analytical techniques, occurrence and health effects of micro and nano plastics deposited in street dust. *Int. J. Environ. Anal. Chem.* **2020**, *102*, 6435–6453. [[CrossRef](#)]
19. Kaya, S.I.; Cetinkaya, A.; Ozkan, S.A. Green analytical chemistry approaches on environmental analysis. *Trends Environ. Anal. Chem.* **2022**, *33*, e00157. [[CrossRef](#)]
20. Zhang, W.Y.; Zhang, Y.Z.; Gong, J.R.; Yang, B.; Zhang, Z.H.; Wang, B.; Zhu, C.C.; Shi, J.Y.; Yue, K.X. Comparison of the suitability of plant species for greenbelt construction based on particulate matter capture capacity, air pollution tolerance index, and antioxidant system. *Environ. Pollut.* **2020**, *263*, 114615. [[CrossRef](#)]
21. Freer-Smith, P.H.; Holloway, S.; Goodman, A. The uptake of particulates by an urban woodland: site description and particulate composition. *Environ. Pollut.* **1997**, *95*, 27–35. [[CrossRef](#)] [[PubMed](#)]
22. Prusty, B.A.K.; Mishra, P.C.; Azeez, P.A. Dust accumulation and leaf pigment content in vegetation near the national highway at Sambalpur, Orissa, India. *Ecotoxicol. Environ. Saf.* **2005**, *60*, 228–235. [[CrossRef](#)]
23. Nowak, D.J.; Crane, D.E.; Stevens, J.C. Air pollution removal by urban trees and shrubs in the United States. *Urban For. Urban Green.* **2006**, *4*, 115–123.
24. Jin, H.Y.; Chen, X.H.; Zhong, R.D.; Liu, M.Y. Influence and prediction of PM_{2.5} through multiple environmental variables in China. *Sci. Total Environ.* **2022**, *849*, 157910. [[CrossRef](#)] [[PubMed](#)]
25. Kinane, S.M.; Montes, C.R.; Zapata, M.; Bullock, B.P.; Cook, R.L.; Mishra, D.R. Influence of environmental variables on leaf area index in loblolly pine plantations. *For. Ecol. Manag.* **2022**, *523*, 120445. [[CrossRef](#)]
26. Sun, X.Y.; Xu, S.; Hua, W.C.; Tian, J.R.; Xu, Y.N. Feasibility study on the estimation of the living vegetation volume of individual street trees using terrestrial laser scanning. *Urban Urban Green* **2022**, *71*, 127553. [[CrossRef](#)]
27. Zhang, Y.L.; Li, S.L.; Fu, X.; Dong, R.C. Quantification of urban greenery using hemisphere-view panoramas with a green cover index. *Ecosyst. Health Sustain.* **2021**, *7*, 1929502. [[CrossRef](#)]
28. Ki, D.; Lee, S. Analyzing the effects of Green View Index of neighborhood streets on walking time using Google Street View and deep learning. *Landsc. Urban Plan.* **2021**, *205*, 103920. [[CrossRef](#)]
29. Dong, W.; Yang, Z.Y. Variation characteristics analysis of the vegetation coverage in Midu county based on Landsat 8 remote sensing image. In Proceedings of the 2nd International Conference on Intelligent Information Processing-IIP'17, Bangkok, Thailand, 17–18 July 2017.
30. Hui, F.M.; Tian, Q.J.; Jin, Z.Y.; Li, H.T. Research on the relationship between vegetation index and leaf area index and its quantitative analysis. *Remote Sens. Inf.* **2003**, *2*, 10–13.
31. Chen, W.B.; Xie, T.; Zheng, J.; Wu, S. The influence of land vegetation on the spatial distribution of PM_{2.5} concentration. *J. Ecol.* **2020**, *40*, 7044–7053.
32. Sun, S.; Li, L.J.; Zhao, W.J.; Qi, M.X.; Tian, X.; Li, S.S. Analysis of variation in air pollution in Beijing, Tianjin and Hebei and its correlation with vegetation index. *Environ. Sci.* **2019**, *40*, 1585–1593.
33. Huang, G.J.; Zhong, J.S.; Ao, C.H. Correlation analysis of the spatial and temporal distribution characteristics of PM_{2.5} and vegetation cover in Liupanshui, Guizhou. *Science. Technol. Eng.* **2020**, *20*, 10965–10972.
34. Suárez-Cáceres, G.P.; Fernández-Cañero, R.; Fernández-Espinosa, A.J.; Rossini-Oliva, S.; Franco-Salas, A.; Pérez-Urrestarazu, L. Volatile organic compounds removal by means of a felt-based living wall to improve indoor air quality. *Atmos. Pollut. Res.* **2021**, *12*, 224–229. [[CrossRef](#)]

35. Srbinovska, M.; Andova, V.; Mateska, A.K.; Krstevska, M.C. The effect of small green walls on reduction of particulate matter concentration in open areas. *J. Clean. Prod.* **2021**, *279*, 123306. [[CrossRef](#)]
36. Pettit, T.; Torpy, F.R.; Surawski, N.C.; Fleck, R.; Irga, P.J. Effective reduction of roadside air pollution with botanical biofiltration. *J. Hazard. Mater.* **2021**, *414*, 125566. [[CrossRef](#)]
37. Doronzo, D.M.; Al-Dousari, A.; Folch, A.; Dagsson-Waldhauserova, P. Preface to the Dust Topical Collection. *Arab. J. Geosci.* **2016**, *9*, 468. [[CrossRef](#)]
38. Subramaniam, N.; Al-Sudairawi, M.; Al-Dousari, A.; Al-Dousari, N. Probability distribution and extreme value analysis of total suspended particulate matter in Kuwait. *Arab. J. Geosci.* **2015**, *8*, 11329–11344. [[CrossRef](#)]
39. Yan, J.; Ji, H.L.; Zhang, Y. Study on the impact of rainfall and flooding on Nanjing Zijinshan National Forest Park based on DEM and NDVI. *J. Anhui Agric. Univ.* **2020**, *47*, 192–199.
40. Wang, Z.B.; Zou, B.; Qiu, Y.H.; Chen, J.W. Geographic characteristics of the spatial and temporal correlation between aerosol optical thickness and PM_{2.5} in China. *Remote Sens. Inf.* **2016**, *31*, 26–35.
41. Nanjing Municipal Bureau Statistics. *Nanjing Statistical Yearbook 2020*; China Statistics Press: Beijing, China, 2020.
42. Gao, L.; Tang, L.; Hou, H.R.; Wang, Y.; Mai, Y.Q.; He, W.B.; Wang, W.M.; Su, H.B. Spatial and temporal distribution of air pollution in Shenzhen and its relationship with landscape patterns. *J. Ecol.* **2021**, *41*, 8758–8770.
43. Wang, Y.H.; Cui, X.; Chen, W. An empirical study on the relationship between economic development and environmental pollution in Nanjing. *Yangtze River Basin Resour. Environ.* **2006**, *2*, 142–146.
44. Yu, Z.H.; Sun, R.L.; Qin, H.X.; Yao, L.P.; Cheng, T.Q. Study on the path of achieving a high quality ecological environment in the Yangtze River Economic Belt with Nanjing as an example. *Yangtze River Basin Resour. Environ.* **2022**, *31*, 379–386.
45. Tan, L. *Research on the Construction of Urban Green Space Landscape Patterns under the Constraints of PM_{2.5} and Evaluating the Construction of Index Systems*; Southwest University: Chongqing, China, 2020.
46. Liu, Y.P.; Wu, J.G.; Yu, D.Y. Characterizing spatiotemporal patterns of air pollution in China: A multiscale landscape approach. *Ecol. Indic.* **2017**, *76*, 344–356. [[CrossRef](#)]
47. Lu, D.B.; Mao, W.L.; Yang, D.Y.; Yang, D.Y.; Zhao, J.N.; Xu, J.H. Effects of land use and landscape pattern on PM_{2.5} in Yangtze River Delta, China. *Atmos. Pollut. Res.* **2018**, *9*, 705–713. [[CrossRef](#)]
48. Zhao, Y.Y.; Zhang, X.P.; Chen, M.X.; Gao, S.S.; Li, R.K. Regional differences and attribution analysis of urban air quality in China. *J. Geogr.* **2021**, *76*, 2814–2829.
49. Li, D.K.; Liu, M.; Li, C.L.; Hu, Y.M.; Wang, C.; Liu, C. Two-and three-dimensional landscape pattern relationships between urban atmospheric environment and surrounding areas in China. *J. Appl. Ecol.* **2021**, *32*, 1593–1602.
50. Liu, Y.Q.; Xu, X.Y.; Huang, M.; Liu, Q. Characteristics of atmospheric PM₁₀, NO₂ and SO₂ concentration changes in Luoyang City. *Soil Water Conserv. Res.* **2018**, *25*, 178–182.
51. Tao, S.C.; Deng, S.X.; Hao, Y.Z.; Gao, S.H.; Xiong, X.Z.; Kong, Y.P. Emission characteristics of gaseous pollutants from road mobile sources in the Guanzhong city group. *China Environ. Sci.* **2019**, *39*, 542–553.
52. Li, W.H.; Zhou, X.; Zhong, J.L. Spatiotemporal differentiation characteristics of ecological protection and high-quality development in Guangxi Zhuang Autonomous Region. *Res. Soil Water Conserv.* **2023**, *30*, 165–174.
53. Ji, Y.U.; Sheng, Q.Q.; Zhu, Z.L. Assessment of ecological benefits of urban green spaces in Nanjing city, China, based on the entropy method and the coupling harmonious degree model. *Sustainability* **2023**, *15*, 10516. [[CrossRef](#)]
54. Xu, P.; Hao, Q.J.; Ji, D.S.; Zhang, J.K.; Liu, Z.R.; Hu, B.; Wang, Y.S.; Jiang, C.S. Characterization of atmospheric PM_{2.5}, NO_x, SO₂ and O₃ concentrations in Beibei, Chongqing. *J. Environ. Sci.* **2016**, *36*, 1539–1547.
55. Shao, P.; Wang, L.L.; An, J.L.; Zhou, Y.L.; Wang, Y.S. Atmospheric pollution observations in Zhangjiakou, Hebei. *Environ. Sci.* **2012**, *33*, 2538–2550.
56. Lei, Y.K.; Davies, G.M.; Jin, H.; Tian, G.H.; Kim, G. Scale-dependent effects of urban greenspace on particulate matter air pollution. *Urban For. Urban Green.* **2021**, *61*, 127089. [[CrossRef](#)]
57. Zheng, C.Y.; Liang, J.H.; Wang, J. Spatial and temporal variation of normalized vegetation index (NDVI) in the China-Pakistan Economic Corridor and analysis of its influencing factors. *J. Ecol. Rural. Environ.* **2022**, *9*, 1147–1156.
58. Wu, W.; Wang, Y.Q.; Liu, M.; Li, C.L. A Review on the Use of Landscape Indices to Study the Effects of Three-Dimensional Urban Landscape Patterns on Haze Pollution in China. *Pol. J. Environ. Stud.* **2021**, *30*, 2957–2967. [[CrossRef](#)]
59. Zang, Z.F.; Zhang, F.Y.; Li, Y.H.; Xing, Y. Spatio-temporal distribution and affecting factors of PM_{2.5} and PM₁₀ in major grain producing areas in China: A case study of Henan province. *J. Nat. Resour.* **2021**, *36*, 1163–1175. [[CrossRef](#)]
60. Li, J.K.; Wang, W.; Li, M.; Li, Q.; Liu, Z.M.; Chen, W.; Wang, Y.A. Impact of land management scale on the carbon emissions of the planting industry in China. *Land* **2022**, *11*, 816. [[CrossRef](#)]
61. Xi, X.; Sokolik, I.N. Quantifying the anthropogenic dust emission from agricultural land use and desiccation of the Aral Sea in Central Asia. *J. Geophys. Res.-Atmos.* **2016**, *121*, 12270–12281. [[CrossRef](#)]
62. Miao, Q.; Wang, Z.S.; Wang, R.; Huang, M.; Sun, J.L. Assessment of the impact of O₃ pollution on summer vegetation growth in Northern China based on NDVI data. *Remote Sens. Technol. Appl.* **2018**, *33*, 696–702.
63. Li, M.W.; Luan, Q.; Zhang, N.; Chang, Q.; Fan, Z.H.; Yang, Q.; Zhao, Y.Q.; Mi, X.N. Analysis of the spatial and temporal dynamics of NDVI and its influencing factors in Luliang from 2000–2019. *Soil Water Conserv. Res.* **2022**, *29*, 248–254.

64. Xu, Y.; Zhao, C.; Dou, S.Q.; Hao, W.Q.; Zheng, Z.W.; Jing, J.L. Spatial and temporal development of NDVI and its correlation with population density in the Bohai Rim from 2000 to 2020. *Soil Water Conserv. Bull.* **2022**, *42*, 264–274.
65. Han, G.F.; Xu, J.H. Spatial and temporal correlation between urbanization and vegetation activity in the Yangtze River Delta. *Ecol. Sci.* **2008**, *27*, 1–5.

Disclaimer/Publisher's Note: The statements, opinions and data contained in all publications are solely those of the individual author(s) and contributor(s) and not of MDPI and/or the editor(s). MDPI and/or the editor(s) disclaim responsibility for any injury to people or property resulting from any ideas, methods, instructions or products referred to in the content.